British Journal of Pharmacology (2008) 155, 934–944

0007–1188/08 $32.00
www.brjpharmacol.org

RESEARCH PAPER

Cytoskeletal toxicity of pectenotoxins in hepatic cells

B Espiña[1], MC Louzao[1], IR Ares[1], E Cagide[1], MR Vieytes[2], FV Vega[2], JA Rubiolo[2], CO Miles[3,4], T Suzuki[5], T Yasumoto[2,6] and LM Botana[1]

[1]*Departamento de Farmacologia, Facultad de Veterinaria, Universidad de Santiago de Compostela, Lugo, Spain;* [2]*Departamento de Fisiologia Animal, Facultad de Veterinaria, Universidad de Santiago de Compostela, Lugo, Spain;* [3]*National Veterinary Institute, PB 8156 Dep., Oslo, Norway;* [4]*AgResearch Ltd, Ruakura Research Centre, Hamilton, New Zealand;* [5]*Tohoku National Fisheries Research Institute, Shinhama, Shiogama, Miyagi, Japan and* [6]*Japan Food Research Laboratories, Tama, Tokyo, Japan*

Background and purpose. Pectenotoxins are macrocyclic lactones found in dinoflagellates of the genus *Dinophysis*, which induce severe liver damage in mice after i.p. injection. Here, we have looked for the mechanism(s) underlying this hepatotoxicity.

Experimental approach. Effects of pectenotoxin (PTX)-1, PTX-2, PTX-2 seco acid (PTX-2SA) and PTX-11 were measured in a hepatocyte cell line with cancer cell characteristics (Clone 9) and in primary cultures of rat hepatocytes. Cell morphology was assessed by confocal microscopy; F- and G-actin were selectively stained and cell viability measured by Alamar Blue fluorescence.

Key results. Clone 9 cells and primary hepatocytes showed a marked depolymerization of F-actin with PTX-1, PTX-2 and PTX-11 (1–1000 nM) associated with an increase in G-actin level. However, morphology was only clearly altered in Clone 9 cells. PTX-2SA had no effect on the actin cytoskeleton. Despite the potent F-actin depolymerizing effect, PTX-1, PTX-2 or PTX-11 did not decrease the viability of Clone 9 cells after 24-h treatment. Only prolonged incubation (>48 h) with PTXs induced a fall in viability, and under these conditions, morphology of both Clone 9 and primary hepatocytes was drastically changed.

Conclusions and implications. Although the actin cytoskeleton was clearly altered by PTX-1, PTX-2 and PTX-11 in the hepatocyte cell line and primary hepatocytes, morphological assessments indicated a higher sensitivity of the cancer-like cell line to these toxins. However, viability of both cell types was not altered.

British Journal of Pharmacology (2008) **155**, 934–944; doi:10.1038/bjp.2008.323; published online 8 September 2008

Keywords: confocal microscopy; filamentous actin; lactone ring; metabolic rate; monomeric actin; pectenotoxin

Abbreviations: F-actin, filamentous actin; G-actin, globular actin; Lat A, latrunculin A; PTX, pectenotoxin; PTX-2SA, pectenotoxin-2 seco acid

Introduction

Pectenotoxins (PTXs) are toxic compounds first isolated from the Japanese scallop, *Patinopecten yessoensis* (Yasumoto *et al*., 1984). Initially, they were classified as DSP toxins in accordance with their origin (dinoflagellates from the genus *Dinophysis*). On the basis of the lack of diarrhoea-like symptoms in mice after oral administration of PTX-2, pectenotoxin-2 seco acid (PTX-2SA) or PTX-11 (Miles *et al*., 2004a; Suzuki *et al*., 2006) and the absence of protein phosphatase inhibition (Luu *et al*., 1993; Fladmark *et al*., 1998), PTXs are nowadays classified as a separate group of phycotoxins.

The liver is an essential detoxifying organ for the majority of animals. Intraperitoneal injection of some PTXs in mice triggers severe liver damage (Terao *et al*., 1986). However, no toxicity was found after oral ingestion (Terao *et al*., 1986; Miles *et al*., 2004a; Suzuki *et al*., 2006). Only by using high doses has some oral toxicity been reported (Ishige *et al*., 1988). Little is known about the mechanism of action of PTXs, but monomeric actin was proposed as the principal target of PTXs (Hori *et al*., 1999) and cytoskeletal F-actin disruption as the main effect at the cellular level (Spector *et al*., 1999; Leira *et al*., 2002; Ares *et al*., 2005, 2007). However, so far there is no information on the simultaneous effect of PTXs on F- and G-actin.

Correspondence: Dr LM Botana, Departamento de Farmacología, Facultad de Veterinaria, Universidad de Santiago de Compostela, Lugo, Veterinaria 27002, Spain.
E-mail: Luis.Botana@usc.es
Received 9 May 2008; revised 13 June 2008; accepted 3 July 2008; published online 8 September 2008

Many studies have reported a higher susceptibility of malignant cells to agents disrupting the cytoskeleton (Stournaras *et al*., 1996; Chae *et al*., 2005). In fact, diverse compounds with F-actin-disrupting effects, such as latrunculins and cytochalasins, have been postulated as potential anticancer compounds (Jordan and Wilson, 1998).

Another effect of PTXs at the cellular level is cytotoxicity and induction of apoptosis, as described in salmon and rat hepatocytes after exposure to PTX-1 or in mouse ovulated oocytes after treatment with PTX-2 (Jung *et al*., 1995; Fladmark *et al*., 1998; Chae *et al*., 2005). However, there are no time-course studies in these reports. In addition, many other PTX analogues are being found (Daiguji *et al*., 1998; Burgess and Shaw, 2001; Miles *et al*., 2004b, 2006a) and comparative studies would therefore be valuable.

As the liver seems to be the target organ of PTXs and the actin cytoskeleton the main cellular target, the goal of this study was to investigate the effects of a range of PTXs on F- and G-actin in two cellular models: Clone 9 rat hepatocytes, a cell line derived from hepatocytes with cancer cell characteristics extensively used previously as hepatic cell model (Louzao *et al*., 2007), and primary rat hepatocytes. The PTXs tested were the major compound of this group (PTX-2), two compounds generated by the metabolism of PTX-2 in bivalves (PTX-1 and PTX-2SA) and a novel homologue (PTX-11). We also tested cytotoxicity by following the viability of cells incubated with these toxins for 24 h.

Materials and methods

Cell culture

Clone 9 rat hepatocytes. Rat hepatocytes from the cell line Clone 9 (ECACC no. 88072203) were grown on 60-mm tissue culture plates in F-12 Ham Kaighn's modification supplemented with 2.5 g L^{-1} $NaHCO_3$, 28 mg L^{-1} streptomycin sulphate salt, 17 mg L^{-1} penicillin G potassium salt and 10% foetal bovine serum, pH 7.2. The hepatocytes were grown in a humidified atmosphere with 5% CO_2 at 37 °C.

Hepatocytes were seeded on coverslips, which were placed in 8-well sterile plates. Coverslips were used when the cells reached confluence.

Isolation and culture of primary rat hepatocytes. All animal procedures complied with our institutional guidelines for animal care and were approved by the Bioethical Committee of the University of Santiago de Compostela. Rat hepatocytes were obtained from adult male Sprague–Dawley rats. Isolation was as described previously (Pazo *et al*., 2002) by the two-step perfusion procedure with 0.025% collagenase Type IV. Viability was tested by Trypan blue exclusion and was always $\geqslant$85%.

Hepatocytes were seeded on coverslips placed in 8-well sterile plates for attachment in minimum essential and 199 media (4:1) supplemented with penicillin (100 IU mL^{-1}), streptomycin (100 μg mL^{-1}), insulin (5 μg mL^{-1}), BSA (1 mg mL^{-1}), dexamethasone (10^{-6} M), 10% foetal bovine serum, and incubated for 4 h at 37 °C and 5% CO_2. Then, the medium was replaced with fresh medium supplemented with 0.6 mM hydrocortisone-21-hemisuccinate (Barbini *et al*., 2006).

F- and G-actin cytoskeleton staining

After incubation with toxins in the culture medium, cells were washed with phosphate-buffered saline and fixed with 4% paraformaldehyde solution (10 min). Then, cells were permeabilized for 5 min with phosphate-buffered saline–0.1% Triton X-100 and incubated with 0.165 μM Oregon Green 514 Phalloidin for F-actin labelling and 0.3 μM Texas Red DNase I for G-actin labelling for 20 min. Coverslips were mounted on slides with 1:1 glycerol–phosphate-buffered saline and sealed with nail varnish to preserve fluorescence and stored at 4 °C. Control cells were incubated in the same conditions with the toxin vehicle, ethanol. The amount of the vehicle added to the cultures never exceeded 0.1% of the total volume of the incubation media.

Confocal microscopy for visualizing morphology, actin cytoskeleton distribution and measuring

Confocal imaging was performed with a $\times$40 oil-immersion objective of a Nikon Eclipse TE2000-E inverted microscope attached to the C1 laser confocal system (EZC1 V.2.20 software; Nikon Instruments, Europe B.V., Amstelveen, The Netherlands). A 488 nm argon laser was used to excite Oregon Green 514 phalloidin and a 546 nm Helio-neon laser for exciting Texas Red DNase I.

Fluorescent images shown as sequential photographs were acquired at 512 $\times$ 512 pixel resolution in the same region but separately for each fluorophore and then mixed to prevent interfaces. We confirmed that Texas Red did not exhibit fluorescence on the green channel when excited with the argon laser and that Oregon Green did not show fluorescence on the red channel when excited with the Helio-neon laser.

Fluorescence measurements corresponding to F- and G-actin labelling were acquired and calculated separately with quantification software from Z-stack sections taken at 0.5-μm intervals. Values from all independent experiments were averaged for a single data point.

Results are presented as the percentage of the mean value ± s.e.mean of fluorescence emitted by cells treated with toxins, versus controls, with $n \geqslant 3$.

Alamar blue assay

Metabolic activity of Clone 9 cells was measured by using Alamar blue. This compound links to the respiratory chain without affecting the integrity of cells (Ahmed *et al*., 1994). When Alamar Blue is reduced, it becomes fluorescent. Thus, cell metabolic rates can be evaluated proportionally with the fluorescence intensity.

Cells (40 000 per well) were seeded on to 96-well plates. After 24 h, PTX-1, PTX-2, PTX-2SA, PTX-11 or vehicle were added to the cells. Then, a 1:10 dilution of Alamar Blue was added. Fluorescence was measured by using a microplate

fluorescence reader FL600 (Bio-Tek, Winooski, VT, USA) after 2, 4, 6, 8, 12 and 24 h of incubation with the toxins. Results are presented as percentage of fluorescence versus control; mean values ± s.e.mean, with $n \geqslant 3$.

Statistical analysis

Results were analysed using the Students's *t*-test for paired data where appropriate. A probability level of $\leqslant 0.05$ was set to indicate statistical significance.

Drug/molecular target nomenclature conforms to *British Journal of Pharmacology's* Guide to Receptors and Channels (Alexander *et al*., 2008)

Materials

Pectenotoxin-11 was isolated from a New Zealand bloom of *Dinophysis acuta* (Suzuki *et al*., 2006) and PTX-2SA was produced enzymatically from PTX-2 isolated from a New Zealand bloom of *D. acuta* (Miles *et al*., 2004a). The PTX-2 used in this study was isolated from a Norwegian bloom of *D. acuta* (Miles *et al*., 2004a). PTX-1 was isolated from Japanese scallops (Yasumoto *et al*., 1989). Latrunculin A (Lat A) derived from *Negombata magnifica* was purchased from Sigma-Aldrich (Madrid, Spain). The fluorescent dye Oregon Green 514 Phalloidin for F-actin labelling and Texas Red DNase I for G-actin labelling were obtained from Molecular Probes (Leiden, The Netherlands). Alamar Blue was purchased from Biosource (Madrid, Spain).

Cell culture reagents: nutrient mixture F-12 Ham Kaighn's modification, streptomycin sulphate salt and penicillin G potassium salt were purchased from Sigma (Madrid, Spain) and foetal porcine serum was purchased from Gibco (Barcelona, Spain). BSA was purchased from ICN Biomedicals Inc. (Ohio, USA). Collagenase Type IV was obtained from Sigma-Aldrich. All other chemicals were of reagent grade and purchased from Sigma-Aldrich or Panreac (Barcelona, Spain).

Results

First, Clone 9 cells and primary cultured hepatocytes were incubated for 3 h with different concentrations of the parental compound, PTX-2 (1, 50, 100, 200, 500 and 1000 nM). Then, F- and G-actin were stained simultaneously. Finally, cell fluorescence was measured by confocal microscopy. In Clone 9 cells, the lowest dose of PTX-2 induces no significant change in the actin cytoskeleton structure or in cell morphology (Figures 1b and f). However, 50 nM PTX-2 was enough to trigger little disorganization of actin cytoskeleton (Figure 1c). Clone 9 cells treated with 100 nM PTX-2 showed generally decreased labelling of F-actin, with some intense fluorescent spots (Figure 1d). The highest concentrations of toxin, 200, 500 and 1000 nM, evoked a marked disappearance of the F-actin fluorescence and a clear increase in that of G-actin (Figure 2a, b and c). The effects of PTX-2 on F-actin and G-actin were dose dependent (Figures 2g and h). In terms of cell morphology, the normal well-extended and leaf-like morphology of Clone 9 hepatocytes was changed progressively to a rounder shape with some projections, from a concentration of 50 nM PTX-2 upwards (Figures 1g, h, d, e and f).

Primary cultured hepatocytes treated with PTX-2, under the same conditions as Clone 9 cells, showed a similar response for F- and G-actin labelling. Neither F- nor G-actin fluorescence was changed in cells treated with the lowest concentration (1 nM) of PTX-2 but, above 50 nM, the disorganization of the actin cytoskeleton was increased. As with Clone 9 cells, the F-actin fluorescence disappeared and that of G-actin increased progressively and dose dependently (Figures 3c, d, 4a, b and c, g and h). However, changes in the morphology of the primary hepatocytes were not as obvious as with the Clone 9 cells (Figures 3f, g, h, 4d, e and f). Only a minor rounding effect was observed with the highest concentrations of PTX-2 (Figures 4e and f).

As a concentration of 200 nM PTX-2 induced a clear effect on the actin cytoskeleton of both types of hepatocyte, we

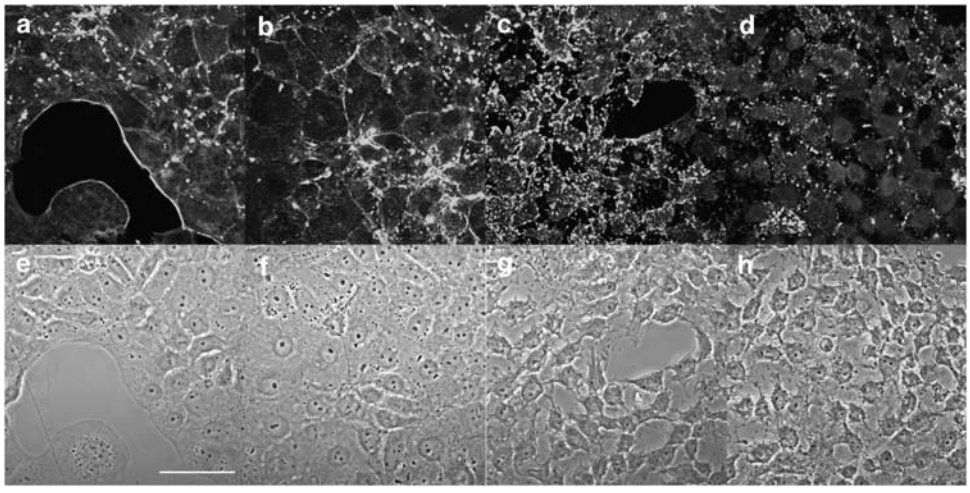

Figure 1 Effects of low concentrations of PTX-2 on the actin cytoskeleton in Clone 9 cells. Confocal imaging of F- and G-actin double-staining of Clone 9 rat hepatocytes showing fluorescence (upper row) and transmission (lower row) images. F- and G-actin were labelled with Oregon Green 514 phalloidin and Texas Red DNase I, respectively. Control cells (**a** and **e**) and Clone 9 cells incubated with 1 nM PTX-2 (**b** and **f**) 50 nM PTX-2 (**c** and **g**) and 100 nM PTX-2 (**d** and **h**). Images are representative of three independent experiments. Digital zoom = × 2. Scale bar = 50 μm.

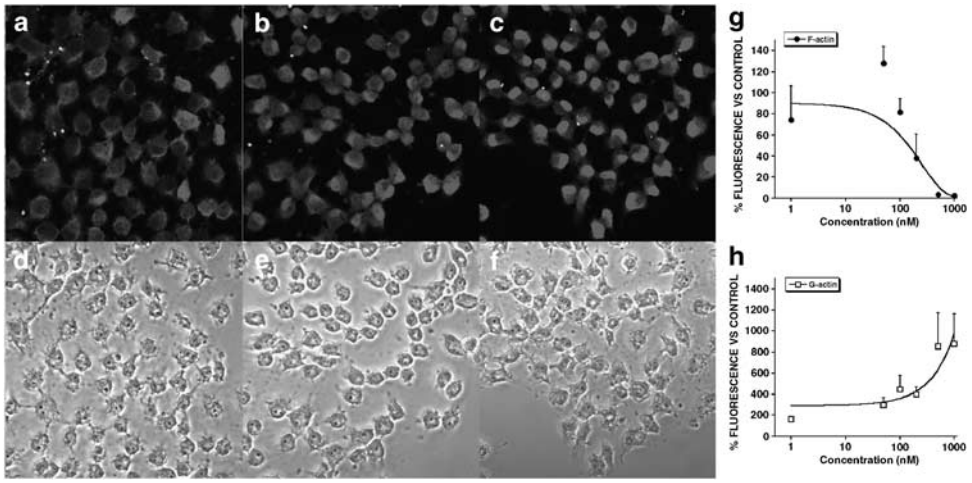

Figure 2 Effects of high concentrations of PTX-2 on the actin cytoskeleton in Clone 9 cells. Confocal imaging of F- and G-actin double-staining of Clone 9 rat hepatocytes showing fluorescence (upper row) and transmission (lower row) images. F- and G-actin were labelled with Oregon Green 514 phalloidin and Texas Red DNase I, respectively. Clone 9 cells incubated with 200 nM PTX-2 (**a** and **d**) 500 nM PTX-2 (**b** and **e**) and 1000 nM PTX-2 (**c** and **f**). Images are representative of three independent experiments. Digital zoom = $\times$ 2. Scale bar = 50 μm. (**g** and **h**) represent dose–response curves of the effect on F- and G-actin of PTX-2 on Clone 9 hepatocytes, respectively. Results are expressed as percentage of fluorescence in cells incubated with PTX-2 versus controls (100%). Mean $\pm$ s.e.mean for $n \geqslant 3$ experiments.

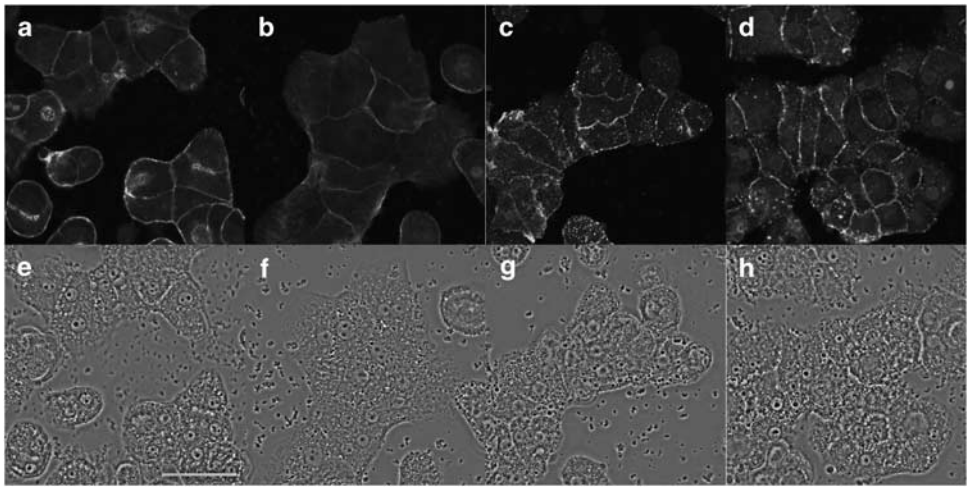

Figure 3 Effects of low concentrations of PTX-2 on the actin cytoskeleton in primary hepatocytes. Confocal imaging of F- and G-actin double-staining of primary rat hepatocytes showing fluorescence (upper row) and transmission (lower row) images. F- and G-actin were labelled with Oregon Green 514 phalloidin and Texas Red DNase I, respectively. Control cells (**a** and **e**) and Clone 9 cells incubated with 1 nM PTX-2 (**b** and **f**) 50 nM PTX-2 (**c** and **g**) and 100 nM PTX-2 (**d** and **h**). Images are representative of three independent experiments. Digital zoom = $\times$ 2. Scale bar = 50 μm.

chose this concentration to carry out a comparative study with the other PTX-2 analogues. Clone 9 cells treated for 3 h with 200 nM PTX-2 and PTX-11 (Figures 5e and i, respectively) showed a clear reduction in fluorescence derived from Oregon Green phalloidin, showing that F-actin levels decreased (Figure 6d), whereas fluorescence from Texas Red DNase I increased, indicating a marked increase in G-actin (Figure 6d). Compared to PTX-2, cells incubated with PTX-1 (Figure 5c) showed a smaller reduction in F-actin content but again G-actin levels increased (Figure 6d). A significant effect was the change in the pattern of F-actin staining, showing a punctate fluorescence (Figure 5c), different from that in control cells (Figure 5a). The metabolite, PTX-2SA (Figure 5g), did not produce any effect on the F-actin cytoskeleton or G-actin (Figure 6d).

Latrunculin A (Lat A), a toxin well known to disrupt F-actin, was also included in these assays. Fluorescence images revealed that Lat A caused F-actin depolymerization with appearance of punctuate structures, very similar to those caused by PTX-1 (Figure 5k), and also increased G-actin (Figure 6d). Cell morphology was assessed by confocal microscopy and showed that Clone 9 cells incubated with PTX-1, PTX-2 and PTX-11 were retracted to the nuclear region and arborized (Figures 5d, f, and j, respectively), an effect similar to that in cells incubated with Lat A (Figure 5l). These morphological changes were more clearly shown in $\times$ 2 zoom images of cells treated with PTX-2 versus controls (Figure 6). It is relevant to point out that PTX-2SA that had no effect on the actin cytoskeleton also did not modify cell morphology (Figure 5h).

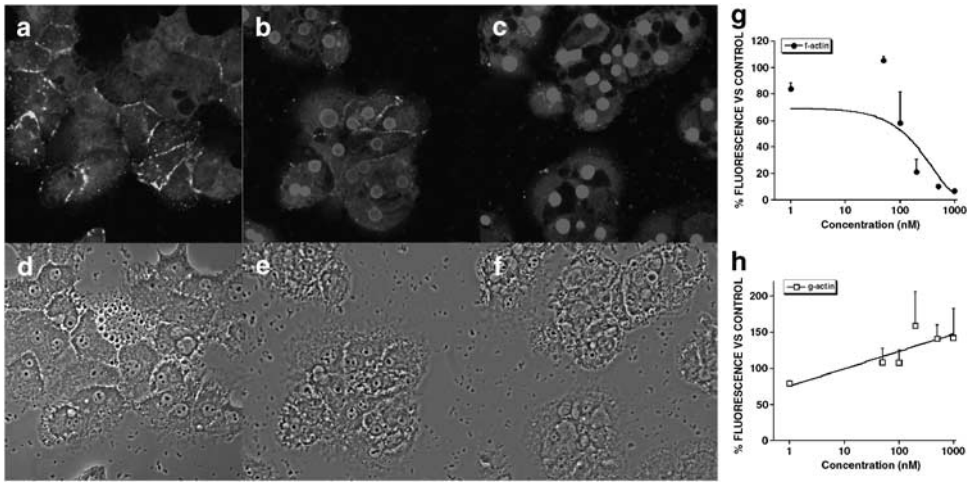

Figure 4 Effects of high concentrations of PTX-2 on the actin cytoskeleton in primary hepatocytes. Confocal imaging of F- and G-actin double-staining of primary rat hepatocytes showing fluorescence (upper row) and transmission (lower row) images. F- and G-actin were labelled with Oregon Green 514 phalloidin and Texas Red DNase I, respectively. Primary hepatocytes incubated with 200 nM PTX-2 (**a** and **d**) 500 nM PTX-2 (**b** and **e**) and 1000 nM PTX-2 (**c** and **f**). Images are representative of three independent experiments. Digital zoom = × 2. Scale bar = 50 μm. (**g** and **h**) represent dose–response curves of the effect on F- and G-actin of PTX-2 on primary hepatocytes, respectively. Results are expressed as percentage of fluorescence in cells incubated with PTX-2 versus controls (100%). Mean ± s.e.mean for $n \geqslant 3$ experiments.

Following the same procedure (incubation with the toxin followed by labelling with the specific fluorescent dyes), images from primary rat hepatocytes are presented in Figure 7. F-actin staining appeared to be disorganized and punctate in cells incubated with 200 nM PTX-1, PTX-2 and PTX-11 for 3 h (Figures 7c, e and i). These toxins produced a sharp reduction in the fluorescence of the Oregon Green phalloidin bound to F-actin, compared with controls (Figure 8d). In those cells, G-actin increased slightly relative to controls (Figures 7a, c, e and i). However, this effect was not as clear as in Clone 9 cells. Again, PTX-2SA induced no effect on the actin cytoskeleton in primary hepatocytes (Figure7g). Surprisingly, 200 nM Lat A produced no significant effect on F- or G-actin in primary rat hepatocytes (Figure 7k). The cell morphology of primary hepatocytes incubated with PTX-1, PTX-2 or PTX-11 (Figures 7d, f and j) was almost unaltered, with only minor irregularities in the cortical actin zone (Figure 8). This was an important difference from the response of Clone 9 cells. As seen in Clone 9 cells, treatment of primary hepatocytes with PTX-2SA induced no morphological effects. However, there was also a lack of morphological effect in primary hepatocytes after incubation with Lat A (Figures 7h and l).

On the basis of the fact that the PTXs tested had a stronger effect on cytoskeletal organization and morphology in the cellular line than in primary rat hepatocytes, we performed viability assays on Clone 9 cells. The goal of these experiments was to investigate possible cytotoxicity, related to the cytoskeletal alterations. Clone 9 rat hepatocytes were incubated with 200 nM PTX-1, PTX-2, PTX-2SA or PTX-11, and their metabolic activity was measured with Alamar Blue. Fluorescence of the cells was continuously measured up to 24 h. PTX-1, PTX-2, PTX-11 and PTX-2 SA produced no effect on cell metabolic rate, suggesting that the viability of Clone 9 hepatocytes was not altered by any of the treatments, including Lat A (Figure 6e).

Finally, long-term viability assays were carried out in both kinds of cells. Clone 9 and primary hepatocytes were incubated for 72 h with 200 nM PTX-1, PTX-2, PTX-2SA and PTX-11 and metabolic activity was measured after 48 and 72 h of incubation. The metabolic rate of Clone 9 and primary hepatocytes was acutely decreased after 48 h of treatment with 200 nM PTX-1, PTX-2 and PTX-11 and even more after 72 h (Figures 9i and j). When Clone 9 cells were treated with 200 nM PTX-2 for 48 h, most of the cells detached from the substrate and the remaining showed seriously altered morphology (Figure 9d). F-actin completely disappeared and G-actin increased (Figure 9b). Surprisingly, primary hepatocytes also had important changes in morphology (Figure 9h), but some F-actin was preserved, without disruption (Figure 9f).

Discussion and conclusions

The actin cytoskeleton is a structure involved in many cellular processes. In cells, there is a dynamic equilibrium between filamentous (polymeric) and globular (monomeric) actin (Knowles and McCulloch, 1992; Pollard and Borisy, 2003; Chu and Voth, 2005; Rubenstein and Wen, 2005). Some well-known compounds such as cytochalasins and latrunculins alter this equilibrium by different mechanisms, with severe consequences for cellular integrity (Stournaras *et al*., 1996; Spector *et al*., 1999).

Histopathological studies have demonstrated that i.p injection of PTX-1 ($1\,mg\,kg^{-1}$) induces macroscopic alterations of the liver, including congestion and finely granulated appearance (Terao *et al*., 1986). Microscopic analysis revealed hepatocyte necrosis in periportal regions of hepatic lobules (Terao *et al*., 1986). The fact that, in the same study, PTX-1 caused no pathological changes in the intestine or other visceral organs placed the PTXs in the group of hepatotoxins.

Because the liver seems to be the target organ for PTXs, and the actin cytoskeleton is important in epithelial cells, we assessed the effect of a range of PTXs on the F-actin/G-actin balance in two hepatocyte models: a cell line derived from rat hepatocytes (Clone 9) and primary cultured rat hepatocytes. Our results indicated a clear disrupting effect of PTX-1, PTX-2 and PTX-11 on the actin cytoskeleton, demonstrated not only by a marked decrease in the level of cellular F-actin, but also by a clear increase in the level of G-actin in Clone 9 cells. So, these compounds altered the F-actin/G-actin balance. These toxins also trigger a remarkable depolymerizing effect on the actin cytoskeleton in neuroblastoma cells (Ares *et al*., 2007), but their effect on G-actin was not determined.

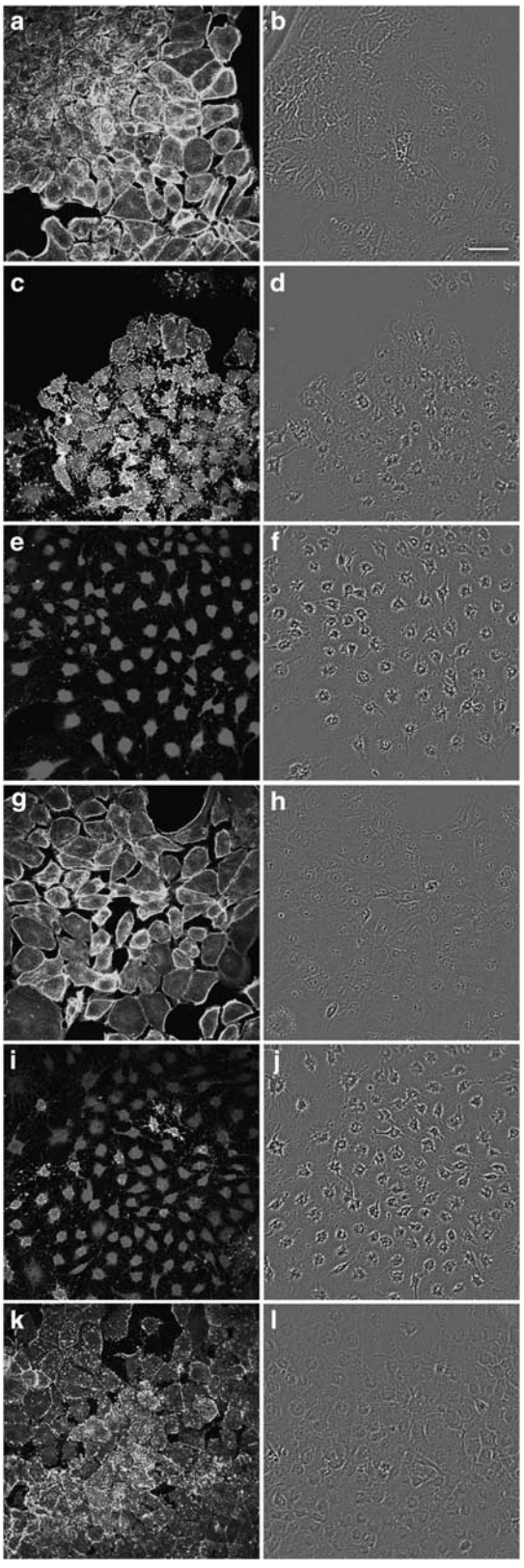

Figure 5 Confocal imaging of F- and G-actin double-staining of Clone 9 rat hepatocytes showing fluorescence (left column) and transmission (right column) images (control and incubated with 200 nM PTXs or Lat A). F- and G-actin were labeled with Oregon Green 514 phalloidin and Texas Red DNase I, respectively. Panels (**a**) and (**b**) show photographs from control cells, while panels (**c**) and (**d**) are from cells treated with PTX-1, (**e** and **f**) with PTX-2, (**g** and **h**) with PTX-2SA, (**i** and **j**) with PTX-11, and (**k** and **l**) with Lat A. Images are representative of three independent experiments. Scale bar = 50 μm.

Many toxins such as cytochalasins, swinholide or jasplakinolide have been reported to modify the F-actin/G-actin balance. These changes are induced by a range of mechanisms of action. Cytochalasins cap the barbed end of F-actin, preventing the incorporation of new actin monomers (Pollard, 1981). Swinholide A binds to monomeric actin and prevents its incorporation in the F-actin chain, but it has also been observed to sever F-actin (Saito *et al*., 1998). Jasplakinolide stabilizes actin filaments and enhances actin nucleation (Spector *et al*., 1999; Bubb *et al*., 2000). Recent *in vitro* studies have shown that although PTX-2 does not sever F-actin, it binds specifically to G-actin between subdomains 1 and 3, and the resulting G-actin–PTX-2 complex appears to cap F-actin at the barbed end (Allingham *et al*., 2007). PTX-1, PTX-2 and PTX-11 could induce cytoskeletal changes in Clone 9 cells by any of these mechanisms, with consequences for cell morphology. Primary rat hepatocytes seemed to be less sensitive to PTXs and displayed scarcely detectable changes in their morphology. Moreover, although PTX-1, PTX-2 and PTX-11 showed F-actin disruption in primary hepatocytes, this effect was weaker than in Clone 9 cells, with no change in G-actin levels. In fact, the punctate pattern of distribution of F-actin points to the degradation of normal F-actin filaments to shorter structures. This could explain the lack of correspondence between a decrease in F-actin fluorescence and the minor increase in G-actin levels. Koch *et al*. (1997) found that C3-like toxin decreased the F-actin content of NIH 3T3 mouse fibroblasts, whereas their G-actin content remained unaltered. They postulated that redistributed actin forms oligomers that were not detected, either as F-actin bundles or as G-actin. In normal hepatocytes, where the effect of cytoskeleton-disrupting agents is decreased, this hypothesis could explain our results.

The PTX metabolite, PTX-2SA, did not induce any effect on the F-actin cytoskeleton or on the shape of cells in any of the cellular models. In addition, our results indicate that in both Clone 9 and rat primary hepatocytes, F- and G-actin levels were unaffected by PTX-2SA. This confirms that integrity of the lactone ring in PTXs is necessary for toxicity (Suzuki *et al*., 2001; Miles *et al*., 2004a, 2006b; Ares *et al*.,

2007) and is in accord with the nature of the PTX-binding site on G-actin (Allingham *et al*., 2007).

Morphological effects of PTXs differed between immortalized and normal rat hepatocytes. Clone 9 cells showed a clear change in shape after incubation with 200 nM PTX-1, PTX-2 and PTX-11, whereas the morphology of primary rat hepatocytes was almost unaltered. Our findings are

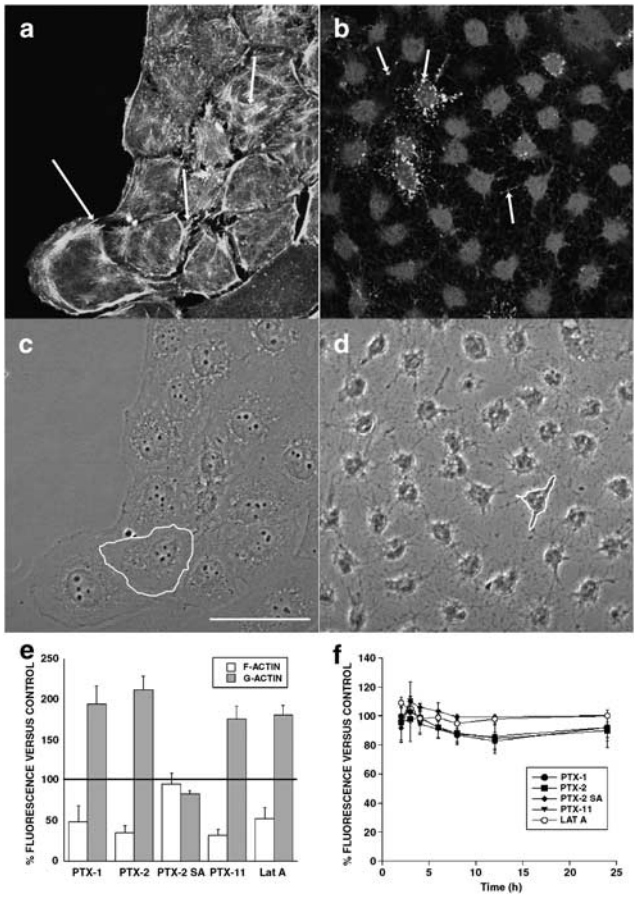

Figure 6 Magnified images of the effects of PTX-2 (200 nM) on the actin cytoskeleton and morphology of Clone 9 cells. Images correspond to $\times 2$ digital zooms. Panels (**a**) and (**c**) are fluorescence and transmission photographs of the control cells, respectively. Panels (**b**) and (**d**) are from cells treated with 200 nM PTX-2. Arrows point to differences on the F-actin distribution between control and treated cells (bundles and dots, respectively). One cell is outlined in controls (**c**) and in cells incubated with PTX-2 (**d**) to show morphological changes. Images are representative of three independent experiments. Scale bar = 50 μm. (**e**) F- and G-actin fluorescence measurements for Clone 9 rat hepatocytes, showing the percentage (mean ± s.e.mean for $n \geqslant 3$ experiments) of fluorescently labeled F- and G-actin in cells treated with PTX-1, PTX-2, PTX-2SA or PTX-11 relative to control cells (100%). (**f**) Viability (mean ± s.e.mean of $n \geqslant 3$ experiments) of Clone 9 cells by Alamar Blue fluorescence after incubation with 200 nM PTXs or Lat A, relative to control cells (100%).

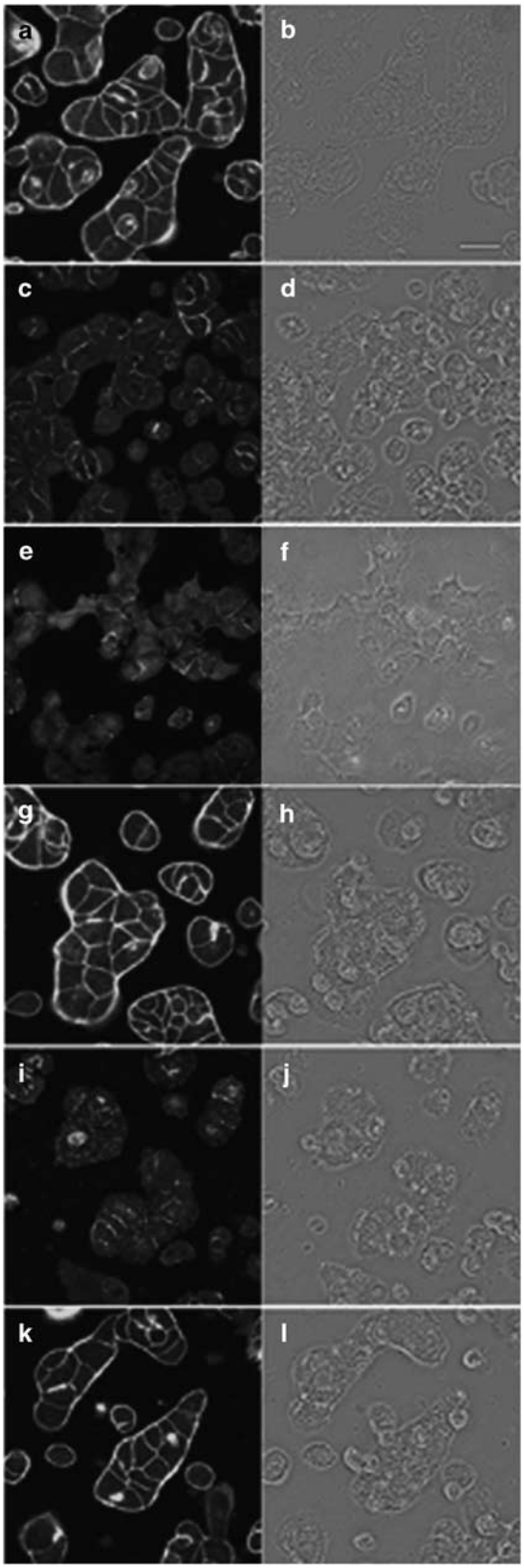

Figure 7 Confocal imaging of F- and G-actin double-staining of primary hepatocytes showing fluorescence (left column) and transmission (right column) images (control and incubated with 200 nM PTXs or Lat A). F- and G-actin were labelled with Oregon Green 514 phalloidin and Texas Red DNase I, respectively. Panels (**a**) and (**b**) show photographs from control cells, whereas panels (**c**) and (**d**) are from cells treated with PTX-1, panels (**e**) and (**f**) with PTX-2, panels (**g**) and (**h**) with PTX-2SA, panels (**i**) and (**j**) with PTX-11, and (**k**) and (**l**) with Lat A. Images are representative of three independent experiments. Scale bar = 50 μm.

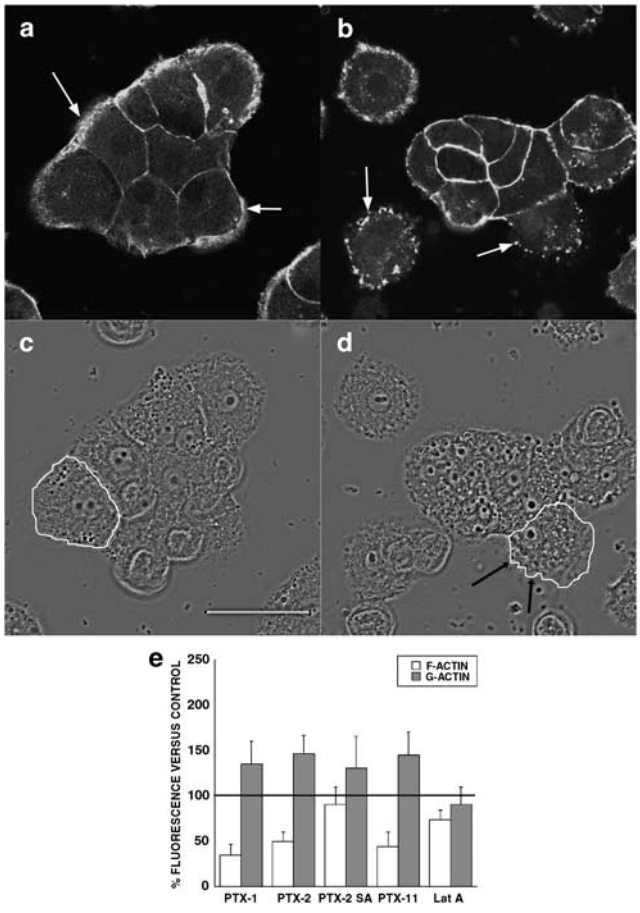

Figure 8 Magnified images of the effects of PTX-2 on the actin cytoskeleton and morphology of primary hepatocytes. Images correspond to $\times 2$ digital zooms. Panels (**a**) and (**c**) are fluorescence and transmission photographs of the control cells, respectively. Panels (**b**) and (**d**) are from cells treated with 200 nM PTX-2. Arrows point to differences on the F-actin distribution between control and treated cells (bundles and dots, respectively). One cell was outlined in controls (**c**) and in cells incubated with PTX-2 (**d**) to show morphological changes. Images are representative of three independent experiments. Scale bar = 50 μm. (**e**) F- and G-actin fluorescence measurements for primary rat hepatocytes, showing the percentage (mean ± s.e.mean for $n \geqslant 3$ experiments) of fluorescently labeled F- and G-actin in cells treated with PTX-1, PTX-2, PTX-2SA or PTX-11 relative to control cells (100%).

compatible with those of Ares *et al.* (2005), using normal, freshly isolated rabbit intestinal cells. The morphology of these cells was not affected by several toxins, including PTX-6, which induced a marked effect on F-actin levels.

Clone 9 hepatocytes are an epithelial cell type. They grow in monolayers, exhibiting contact inhibition as do normal hepatocytes, but are undifferentiated and unpolarized (Weinstein *et al.*, 1975). On the other hand, primary hepatocytes, after isolation, seeding and fixation to the substrate, maintain junctional complexes with other cells, where strong bundles of F-actin are positioned. Thus, Clone 9 cells and primary cultured hepatocytes have structural and morphological differences.

Clone 9 is an immortalized cell line and so they multiply continuously. Two of the hallmarks of tumorigenesis are as follows: (a) an increased rate of proliferation and (b) limitless replicative potential (Hanahan and Weinberg, 2000). Chae *et al* (2005) demonstrated that loss of *p53*, a gene inactivated in the majority of human cancers, sensitized tumours to actin damage by agents such as PTX-2. Although p53 is not inactivated in Clone 9 cells, hypermethylation on DNA cytosine was found in this cell line, and epigenetic DNA cytosine methylation is believed to be one of the root causes of cancer (Asada *et al.*, 2006).

A difference in sensitivity towards actin-depolymerizing agents in immortalized and normal cells has been previously documented with other drugs such as cytochalasin B, where malignant lymphocytes exhibited a higher sensitivity to this compound than did normal lymphocytes (Stournaras *et al.*, 1996). Namba *et al* (1987) found a significant difference in distribution and number of F-actin fibers between immortal and normal fibroblasts. Three immortally transformed fibroblast lines showed a striking reduction in the number and an altered pattern of organization of actin fibers. On the other hand, in normal fibroblasts, actin fibers ran parallel to each other along the long axis of the cells. Such differences in actin could account for the different responses to depolymerizing agents.

Lat A is a well-known G-actin sequestering macrolide that binds to G-actin with a 1:1 stoichiometry (Yarmola *et al.*, 2000). This compound is a good tool to compare F-actin-disrupting agents because its union to monomeric actin is very specific and it does not exert severing or capping activity (Spector *et al.*, 1999; Yarmola *et al.*, 2000). In our experiments, 200 nM Lat A induced an F-actin-disrupting effect comparable with the same concentration of PTX-1 on Clone 9 cells. The lack of activity of 200 nM Lat A in primary hepatocytes points to a lower potency of this compound in normal cells, confirmed by the fact that at concentrations 10-fold higher (2 μM), Lat A induced effects on the actin cytoskeleton equivalent to those of 200 nM PTX-1 (data not shown). Differences in potency could be also related to different actions, for instance, Lat A does not sever or cap F-actin, but PTX-2 showed capping action in addition to the G-actin sequestering effect (Allingham *et al.*, 2007).

Previous studies have shown that cancerous and non-mature (undifferentiated) cells have weaker actin cytoskeletons than normal cells, consistent with the greater effect of F-actin-disrupting agents on cancerous and non-mature cell lines (Stournaras *et al.*, 1996; Jordan and Wilson, 1998), and this may explain the difference in susceptibility of Clone 9 cells and rat primary hepatocytes towards PTXs reported in this article.

Recent studies using other cellular models have investigated the effects of PTXs on apoptosis (Fladmark *et al.*, 1998; Chae *et al.*, 2005). Fladmark *et al.* described apoptosis in primary rat and salmon hepatocytes induced by exposure to 2 μM PTX-1 for 1 h. However, despite the marked effect on cytoskeletal integrity, we observed no significant change in the metabolic rate of Clone 9 rat hepatocytes incubated with 200 nM PTX-1, PTX-2, PTX-2SA or PTX-11 for 24 h, indicating no loss of viability of these cells during the treatments and pointing to the cytoskeletal disruption by PTXs as the primary action on cellular integrity. In longer-term treatments (48–72 h), metabolic rate declined acutely in Clone 9 cells as well as in primary hepatocytes and morphological

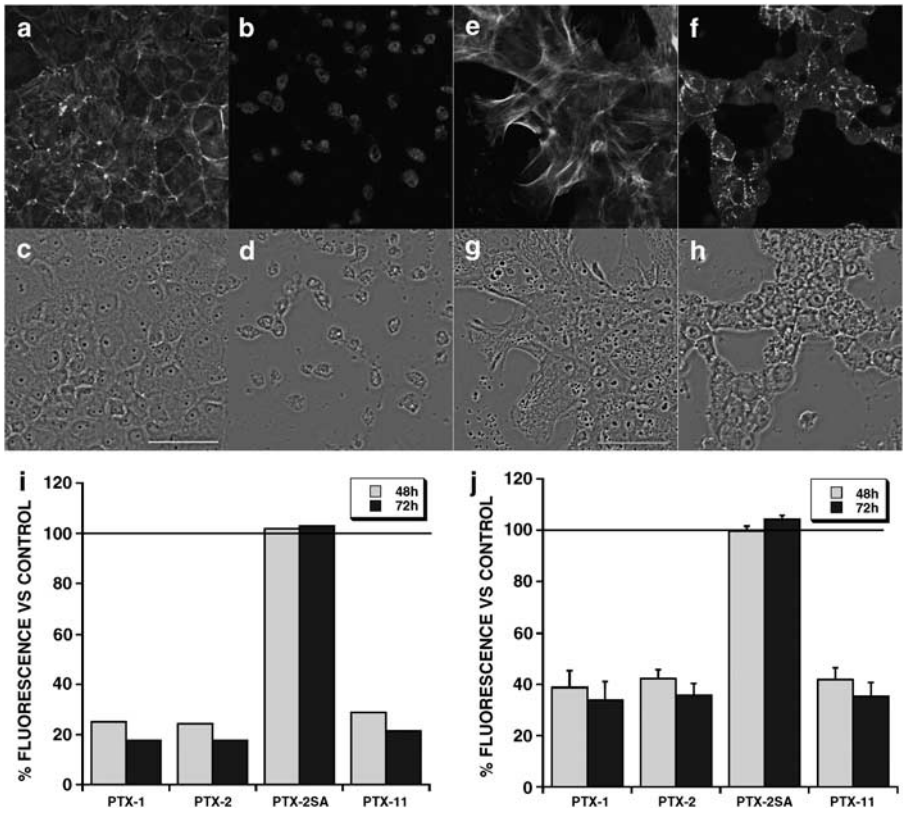

Figure 9 Effect of prolonged treatment with 200 nM PTX-1, PTX-2, PTX-2SA and PTX-11 on the viability and actin cytoskeleton of Clone 9 and primary hepatocytes. Panels (**a**) and (**c**) shows fluorescence and transmission photographs of F- and G-actin of control Clone 9 cells. Panels (**b**) and (**d**) are from Clone 9 cells treated for 48 h with 200 nM PTX-2. Panels (**e**) and (**f**) show fluorescence and transmission photographs of F- and G-actin of control primary hepatocytes. Panels (**g**) and (**h**) are from primary hepatocytes treated for 48 h with 200 nM PTX-2. Photographs are $\times 2$ digital zoom images. Scale bar = 50 μm. Viability was assessed by Alamar Blue fluorescence after incubation of Clone 9 cells or primary hepatocytes (**i** and **j**, respectively) for 48 and 72 h with 200 nM PTXs relative to control cells (100%) (mean ± s.e.mean of $n \geqslant 3$ experiments).

changes appeared in both cell types. But rounding of normal hepatocytes did not correlate, over time, with total disruption of the F-actin cytoskeleton. In fact, the existence of small F-actin bundles suggests that this cytoskeletal effect is closer to that of the shorter time (24 h) treatments. So, the rounding and fall in metabolic rate could be attributed to other, later effects, such as some stage in the apoptotic process. Primary hepatocytes maintained more than 24 h in culture normally acquire flattened and extended morphologies. Tuschl and Mueller (2006) found that after 72 h in culture, there was a marked change in cell morphology; the hepatocytes spread out, nuclear volume was increased and the cytoplasm appeared granulated. Such time-related changes make the rounding effect of PTXs much more evident, after the longer-term incubations.

In conclusion, although PTX-1, PTX-2 and PTX-11 were clearly demonstrated to be F-actin-disrupting agents, they exerted differential effects on immortalized and normal rat hepatocytes at the morphological level. Primary hepatocytes were more resistant to changes in cellular shape induced by these PTXs. In addition, morphological and cytoskeletal effects of PTXs in Clone 9 cells were not correlated with changes in cellular viability after 24 h of treatment. Longer-term exposures induced decreased viability in normal and immortal hepatocytes, accompanied by rounding of their morphology. These effects could be attributed to later processes, initiated by the earlier damage to the actin cytoskeleton. The discovery of differences in the effects of actin-disrupting agents between cells with cancer characteristics and normal cells could be of great clinical importance for the development of new cancer chemotherapy agents.

Acknowledgements

This work was funded by the following grants: contract grant sponsor: Ministerio de Ciencia y Tecnología, Spain; contract grant numbers: AGL2006-08439/ALI, AGL2005-23689-E, AGL2005-23687-E, AGL2004-08268-C02-02/ALI, AGL2007-60946/ALI, REN2003-06598-C02-01. Contract grant sponsor: Xunta de Galicia, Spain; contract grant numbers: GRC 30/2006, PGIDIT05PXIC26101PM, PGIDIT05PXIC26102PM, PGIDIT05PXIC26102PN, PGIDIT04TAL261005PR, PGIDIT 07MMA006261PR and PGIDT07CSA012261PR. EU VIth Frame Program; Grant Number: IP FOOD-CT-2004-06988 (BIOCOP), STREP FOOD-CT-2004-514055 (DETECTOX) and CRP 030270-2 (SPIES-DETOX). Parts of this work were also supported by New Zealand Foundation for Research, Science and Technology contracts CAWX0301 and C10X0406 (International Investment Opportunities Fund), Norwegian Research Council grant 139593/140, and by the BIOTOX project (partly funded by the European Commission,

through 6th Framework Programme contract no. 514074, topic Food Quality and Safety). We thank P Hovgaard, V Beuzenberg and AL MacKenzie for collection of algae from which PTX-2, PTX-2SA and PTX-11 were isolated, and AD Hawkes, M Sandvik, IA Samdal and T Rundberget for assistance with isolation of these compounds.

Conflict of interest

The authors state no conflict of interest.

References

Ahmed SA, Gogal Jr RM, Walsh JE (1994). A new rapid and simple non-radioactive assay to monitor and determine the proliferation of lymphocytes: an alternative to [3H]thymidine incorporation assay. *J Immunol Methods* **170**: 211–224.

Alexander SP, Mathie A, Peters JA (2008). Guide to Receptors and Channels (GRAC), 3rd edition. *Br J Pharmacol* **153** (Suppl 2): S1–S209.

Allingham JS, Miles CO, Rayment I (2007). A structural basis for regulation of actin polymerization by pectenotoxins. *J Mol Biol* **371**: 959–970.

Ares IR, Louzao MC, Espina B, Vieytes MR, Miles CO, Yasumoto T *et al.* (2007). Lactone ring of pectenotoxins: a key factor for their activity on cytoskeletal dynamics. *Cell Physiol Biochem* **19**: 283–292.

Ares IR, Louzao MC, Vieytes MR, Yasumoto T, Botana LM (2005). Actin cytoskeleton of rabbit intestinal cells is a target for potent marine phycotoxins. *J Exp Biol* **208**: 4345–4354.

Asada K, Asada R, Yoshiji H, Fukui H, Floyd RA, Kotake Y (2006). DNA cytosine methylation profile in various cancer-related genes is altered in cultured rat hepatocyte cell lines as compared with primary hepatocytes. *Oncol Rep* **15**: 1241–1248.

Barbini L, Gonzalez R, Dominguez F, Vega F (2006). Apoptotic and proliferating hepatocytes differ in prothymosin alpha expression and cell localization. *Mol Cell Biochem* **291**: 83–91.

Bubb MR, Spector I, Beyer BB, Fosen KM (2000). Effects of jasplakinolide on the kinetics of actin polymerization. An explanation for certain *in vivo* observations. *J Biol Chem* **275**: 5163–5170.

Burgess V, Shaw G (2001). Pectenotoxins—an issue for public health: a review of their comparative toxicology and metabolism. *Environ Int* **27**: 275–283.

Chae HD, Choi TS, Kim BM, Jung JH, Bang YJ, Shin DY (2005). Oocyte-based screening of cytokinesis inhibitors and identification of pectenotoxin-2 that induces Bim/Bax-mediated apoptosis in p53-deficient tumors. *Oncogene* **24**: 4813–4819.

Chu JW, Voth GA (2005). Allostery of actin filaments: molecular dynamics simulations and coarse-grained analysis. *Proc Natl Acad Sci USA* **102**: 13111–13116.

Daiguji M, Satake M, James KJ, Bishop AG, MacKenzie L, Naoki H *et al.* (1998). Structures of new pectenotoxin analogs, pectenotoxin-2 seco acid and 7-epi-2 seco acid, isolated from a dinoflagelate and greenshell mussels. *Chem Lett* **7**: 653–654.

Fladmark KE, Serres MH, Larsen NL, Yasumoto T, Aune T, Doskeland SO (1998). Sensitive detection of apoptogenic toxins in suspension cultures of rat and salmon hepatocytes. *Toxicon* **36**: 1101–1114.

Hanahan D, Weinberg RA (2000). The hallmarks of cancer. *Cell* **100**: 57–70.

Hori M, Matsuura Y, Yoshimoto R, Ozaki H, Yasumoto T, Karaki H (1999). [Actin depolymerizing action by marine toxin, pectenotoxin-2]. *Nippon Yakurigaku Zasshi* **114** (Suppl 1): 225P–229P.

Ishige M, Satoh N, Yasumoto T (1988). Pathological studies on the mice admisnistration with the causative agent of diarrhetic shellfish poisoning (okadaic acid and pectenotoxin-2). *Hokkaidoritsu Eisei Kenkyushoho* **38**: 15–18.

Jordan MA, Wilson L (1998). Microtubules and actin filaments: dynamic targets for cancer chemotherapy. *Curr Opin Cell Biol* **10**: 123–130.

Jung JH, Sim CJ, Lee CO (1995). Cytotoxic compounds from a two-sponge association. *J Nat Prod* **58**: 1722–1726.

Knowles GC, McCulloch CA (1992). Simultaneous localization and quantification of relative G and F actin content: optimization of fluorescence labeling methods. *J Histochem Cytochem* **40**: 1605–1612.

Koch G, Benz C, Schmidt G, Olenik C, Aktories K (1997). Role of Rho protein in lovastatin-induced breakdown of actin cytoskeleton. *J Pharmacol Exp Ther* **283**: 901–909.

Leira F, Cabado AG, Vieytes MR, Roman Y, Alfonso A, Botana LM *et al.* (2002). Characterization of F-actin depolymerization as a major toxic event induced by pectenotoxin-6 in neuroblastoma cells. *Biochem Pharmacol* **63**: 1979–1988.

Louzao MC, Espina B, Vieytes MR, Vega FV, Rubiolo JA, Baba O *et al.* (2007). 'Fluorescent glycogen' formation with sensibility for *in vivo* and *in vitro* detection. *Glycoconj J* **25**: 503–510.

Luu HA, Chen DZ, Magoon J, Worms J, Smith J, Holmes CF (1993). Quantification of diarrhetic shellfish toxins and identification of novel protein phosphatase inhibitors in marine phytoplankton and mussels. *Toxicon* **31**: 75–83.

Miles CO, Wilkins AL, Hawkes AD, Jensen DJ, Selwood AI, Beuzenberg V *et al.* (2006a). Isolation and identification of pectenotoxins-13 and -14 from *Dinophysis acuta* in New Zealand. *Toxicon* **48**: 152–159.

Miles CO, Wilkins AL, Munday JS, Munday R, Hawkes AD, Jensen DJ *et al.* (2006b). Production of 7-epi-pectenotoxin-2 seco acid and assessment of its acute toxicity to mice. *J Agric Food Chem* **54**: 1530–1534.

Miles CO, Wilkins AL, Munday R, Dines MH, Hawkes AD, Briggs LR *et al.* (2004a). Isolation of pectenotoxin-2 from *Dinophysis acuta* and its conversion to pectenotoxin-2 seco acid, and preliminary assessment of their acute toxicities. *Toxicon* **43**: 1–9.

Miles CO, Wilkins AL, Samdal IA, Sandvik M, Petersen D, Quilliam MA *et al.* (2004b). A novel pectenotoxin, PTX-12, in *Dinophysis* spp. and shellfish from Norway. *Chem Res Toxicol* **17**: 1423–1433.

Namba M, Karai M, Kimoto T (1987). Comparison of major cytoskeletons among normal human fibroblasts, immortal human fibroblasts transformed by exposure to Co-60 gamma rays, and the latter cells made tumorigenic by treatment with Harvey murine sarcoma virus. *Exp Gerontol* **22**: 179–186.

Pazo JA, Rodriguez ME, Vega F, De la Cruz L, Guibert E, Mediavilla MG *et al.* (2002). Hepatocytes after cold storage in University of Wisconsin Solution: a tool to study the effects of hypothermic preservation. *Cell Preserv Technol* **1**: 189–199.

Pollard TD (1981). Cytoplasmic contractile proteins. *J Cell Biol* **91**: 156s–165s.

Pollard TD, Borisy GG (2003). Cellular motility driven by assembly and disassembly of actin filaments. *Cell* **112**: 453–465.

Rubenstein PA, Wen KK (2005). Lights, camera, actin. *IUBMB Life* **57**: 683–687.

Saito SY, Watabe S, Ozaki H, Kobayashi M, Suzuki T, Kobayashi H *et al.* (1998). Actin-depolymerizing effect of dimeric macrolides, bistheonellide A and swinholide A. *J Biochem (Tokyo)* **123**: 571–578.

Spector I, Braet F, Shochet NR, Bubb MR (1999). New anti-actin drugs in the study of the organization and function of the actin cytoskeleton. *Microsc Res Tech* **47**: 18–37.

Stournaras C, Stiakaki E, Koukouritaki SB, Theodoropoulos PA, Kalmanti M, Fostinis Y *et al.* (1996). Altered actin polymerization dynamics in various malignant cell types: evidence for differential sensitivity to cytochalasin B. *Biochem Pharmacol* **52**: 1339–1346.

Suzuki T, Mackenzie L, Stirling D, Adamson J (2001). Pectenotoxin-2 seco acid: a toxin converted from pectenotoxin-2 by the New Zealand Greenshell mussel, *Perna canaliculus*. *Toxicon* **39**: 507–514.

Suzuki T, Walter JA, LeBlanc P, MacKinnon S, Miles CO, Wilkins AL *et al.* (2006). Identification of pectenotoxin-11 as 34S-hydroxy-pectenotoxin-2, a new pectenotoxin analogue in the toxic dinoflagellate *Dinophysis acuta* from New Zealand. *Chem Res Toxicol* **19**: 310–318.

Terao K, Ito E, Yanagi T, Yasumoto T (1986). Histopathological studies on experimental marine toxin poisoning. I. Ultrastructural changes in the small intestine and liver of suckling mice induced by dinophysistoxin-1 and pectenotoxin-1. *Toxicon* **24**: 1141–1151.

Tuschl G, Mueller SO (2006). Effects of cell culture conditions on primary rat hepatocytes-cell morphology and differential gene expression. *Toxicology* **218**: 205–215.

Weinstein IB, Orenstein JM, Gebert R, Kaighn ME, Stadler UC (1975). Growth and structural properties of epithelial cell cultures established from normal rat liver and chemically induced hepatomas. *Cancer Res* **35**: 253–263.

Yarmola EG, Somasundaram T, Boring TA, Spector I, Bubb MR (2000). Actin-latrunculin A structure and function. Differential modulation of actin-binding protein function by latrunculin A. *J Biol Chem* **275**: 28120–28127.

Yasumoto T, Murata M, Lee J (1989). Polyether toxins produced by dinoflagellates. In: Natori S, Hashimoto K, Ueno Y (eds). *Mycotoxins and Phycotoxins'88*. Elsevier: Amsterdam, pp 375–382.

Yasumoto T, Murata M, Oshima Y, Matsumoto GK, Clardy J (1984). Diarrhetic shellfish poisoning. In: Ragelis EP (ed). *Seafood Toxins*. American Chemical Society: Washington, DC, pp 207–214.